Chapter 4

Alternating *syn-anti* bacteriochlorophyll *d* forms concentric helical nanotubes in chlorosomes

Chlorosomes are the largest light-harvesting antennae found in nature and could serve as a development platform for supramolecular (opto)electronic and solar energy conversion devices. They contain up to 250,000 BChl molecules in self-organized, heterogeneous structures that cannot be solved by X-ray diffraction. With a combination of EM, NMR and modeling the structure between the molecular and supramolecular levels of well-defined, extended chlorosomes from a *C. tepidum* mutant that synthesizes primarily 17^2-farnesyl-*R*-[E,M] BChl *d* is determined. Distance constraints from solid-state NMR measurements of uniformly ^{13}C-enriched chlorosome preparations and DFT modeling showed that alternating BChl *d* molecules form *syn-anti* monomer stacks. Using structural constraints from cryo-EM, we showed that the stacks self-assemble into coaxial cylinders to form nanotubes from rings perpendicular to the tube axis. The structural model for the mutant provides the conceptual framework to understand the more complex compositional and structural heterogeneity of BChl *c* organization in WT chlorosomes.

4.1 Introduction

Nature has developed a class of elegant, supramolecular nanotube systems for ultrafast, directional energy transfer in the chlorosomes, which are the principal light-harvesting apparatus of green sulfur bacteria, some green filamentous anoxygenic phototrophs, and the recently discovered aerobic anoxygenic phototroph *Candidatus* Chloracidobacterium thermophilum [1,2]. Chlorosomes are elongated sacs containing self-assembled BChl, which differ from other antenna complexes by their very large size (~150 × 60 nm) and the absence of a protein matrix to support the photosynthetic pigments [1,3,4]. Up to 250,000 BChls are organized into active supramolecular light-harvesting devices with strongly red-shifted absorption bands and extremely large exciton diffusion lengths that cover up to 200 BChl monomers [5]. Chlorosomes are efficient light harvesters that are remarkably stable against photodegradation due to self-protection of the BChl from singlet oxygen [1,6]. They can form under extreme environmental conditions and can operate efficiently at very low light intensities to produce ultra-rapid energy transfer [7-10].

The optical and excitonic properties are unprecedented for any other known material and chlorosomes may provide a basis for the design of biomimetic, self-assembling and self-repairing structures for artificial photosynthesis and molecular electronics [11-13]. However, chlorosomes are heterogeneous mixtures built from BChl *c*, *d* or *e* with different side chains and stereochemistry. For instance, the natural chlorosomes of the green sulfur bacterium *C. tepidum* contain BChl *c* molecules with variable degrees of methylation at carbons C-8^2 and C-12^1 and both *R*- and *S*-chirality at carbon C-3^1 [1,14]. In spite of intensive study and extensive debate, the precise arrangement of the pigments in chlorosomes has remained elusive. Conflicting models have been derived from spectroscopic and electron microscopic assessments [15-19].

Recent advances in understanding the biosynthesis of BChl *c* has led to a well characterized *bchQRU*, *C. tepidum* triple mutant, which synthesizes a remarkably homogeneous chlorosome species that principally contains

17²-farnesyl-*R*-[E,M] BChl *d* [14,20]. Both NMR and cryo-EM studies have shown that the *bchQRU* mutant produces very homogeneous chlorosomes with high structural order [17,21]. The BChl *d* molecules form tubular-shaped elements >10 nm in diameter. These nanotubes are apparently formed from coaxial tubes and curved sheets with a separation of 2.1 nm between layers [22,23].

The homogeneity and the higher structural order of chlorosomes from the *bchQRU* mutant provided very high resolution MAS solid-state NMR data that facilitated both the assignment and resolution of distance constraints. When combined with cryo-EM and molecular modeling, this allowed for resolving the structure of a member of the class of chlorosomal antennae, since it was determined that alternating *syn-anti* BChl *d* molecules form supramolecular helical nanotubes.

4.2 Experimental section

4.2.1 Sample preparation

Cells of *C. tepidum* WT, and the *bchQRU* triple mutant strain described in Gomez *et al.* were grown as described in Balaban *et al.* [16,24]. The method for preparation of ^{13}C enriched chlorosomes and the BChl purification are described previously [16,25]. The pigments from the chlorosomes of the *bchQRU* mutant were also isolated and analyzed following the methods described in Steensgaard *et al.* and more than 95% of 17²-farnesyl-*R*-[E,M] BChl *d* was found to be present [25].The chlorosomes samples were kept in the dark at ~4°C.

4.2.2 NMR measurements

All solid-state, MAS NMR experiments were performed with a Bruker AV-750 spectrometer equipped with a 4-mm triple resonance MAS probe head (Bruker, Karlsruhe, Germany), using a ^{13}C radio frequency of 188.6 MHz and a sample temperature of 277 K. Spinning frequencies of 11 kHz ± 5 Hz and 13 kHz ± 5 Hz were used for 2D ^{13}C-^{13}C homo and ^{1}H-^{13}C heteronuclear correlation experiments, respectively. The ^{1}H spins were decoupled during acquisition using the TPPM scheme in all experiments

[26]. 2D ^{13}C-^{13}C dipolar correlation spectra were recorded using the RFDR sequence with simulated phase-sensitive detection in ω_1 at mixing times of 1.4 ms, 2.9 ms and 5.1 ms [27]. A ^{1}H 90° pulse length of 3.1 µs was used with cross-polarization periods of 2 ms. For each of the 256 steps in the indirect dimension, 128 scans were collected. 2D ^{13}C-^{13}C spectra were recorded using the CHHC sequence for indirect detection of ^{1}H-^{1}H contacts at ^{1}H diffusion times of 250 µs and 325 µs [28,29]. The initial CP contact time was set to 256 µs. Short CP contact times of 128 µs enclosing the ^{1}H-^{1}H spin diffusion step were used to ensure that the polarization transfer was restricted to directly bonded ^{1}H-^{13}C spin pairs. For each of the 256 steps in the indirect dimension, 128 scans were collected. A 2D ^{1}H-^{13}C heteronuclear correlation dataset was obtained by using the FSLG experiment, by using a short CP time of 256 µs and a ^{1}H 90° pulse of 3.1 µs [30]. The ^{1}H chemical shift scale was calibrated from a FSLG spectrum of solid tyrosine·HCl salt. For each of 256 steps in the indirect ^{1}H dimension, 128 ^{13}C scans were accumulated.

The ^{13}C and ^{1}H shifts in solution ($\sigma_{liq}^{C}, \sigma_{liq}^{H}$), were determined with 2D ^{13}C-^{13}C COSY, ^{1}H-^{1}H COSY and ^{1}H-^{13}C HSQC NMR spectra of the monomer in CD_2Cl_2 with 5% CD_3OD recorded on a DMX-600 spectrometer (Bruker, Karlsruhe, Germany). The chemical shifts were used to determine the aggregation shifts $\Delta\sigma_i^C = \sigma_i^C - \sigma_{liq}^C$ and $\Delta\sigma_i^H = \sigma_i^H - \sigma_{liq}^H$ for ^{13}C and ^{1}H.

4.2.3 Cryo-EM measurements

Cryo-EM measurements were performed at the Groningen Biomolecular Sciences and Biotechnology Institute and will be described extensively elsewhere [22,31]. Briefly, aliquots of purified chlorosomes were applied to holey carbon grids with a thin layer of carbon and were plunge-frozen in liquid ethane at 83 K with a Vitrobot vitrification system (FEI, Eindhoven, The Netherlands). Electron microscopy was performed with a Tecnai G2 Polara electron microscope (FEI, Eindhoven, The Netherlands) equipped with a Gatan energy filter at 115,000× magnification and a specimen temperature of 80 K. Images were recorded in the zero-loss imaging mode, using a slit-width of 20 eV, with a slow-scan CCD camera at 1 µm underfocus, to have optimal phase contrast transfer at 300 kV for details

with a periodicity of about 2 nm. EM images were simulated as projected electron density from atomic coordinates at 0.6 nm resolution using the EMAN pdb2mrc program [32].

4.2.4 Structure modeling and ring-current calculation

Modeling of the structures listed in Table 4.2 was performed using Hyperchem version 7 software (Hypercube, Inc.). All geometry optimizations used an MM+ force field with a Polak-Ribiere conjugate gradient algorithm with a gradient convergence criterion of 0.01 kcal/mol. DFT calculations were performed using the Gaussian 03 software package and the BLYP exchange-correlation function, which has been used before to estimate NMR shifts for Chl systems [33-36]. The 6-311++G(d,p) Gaussian basis set was used. To calculate the magnetic shielding due to the local magnetic field induced by the ring current effect in the BChls, nucleus-independent chemical shift (NICS) quantum mechanical calculations were performed [37]. Ring-current shifts were calculated using the Gauge-Independent Atomic Orbital (GIAO) method [38-40].

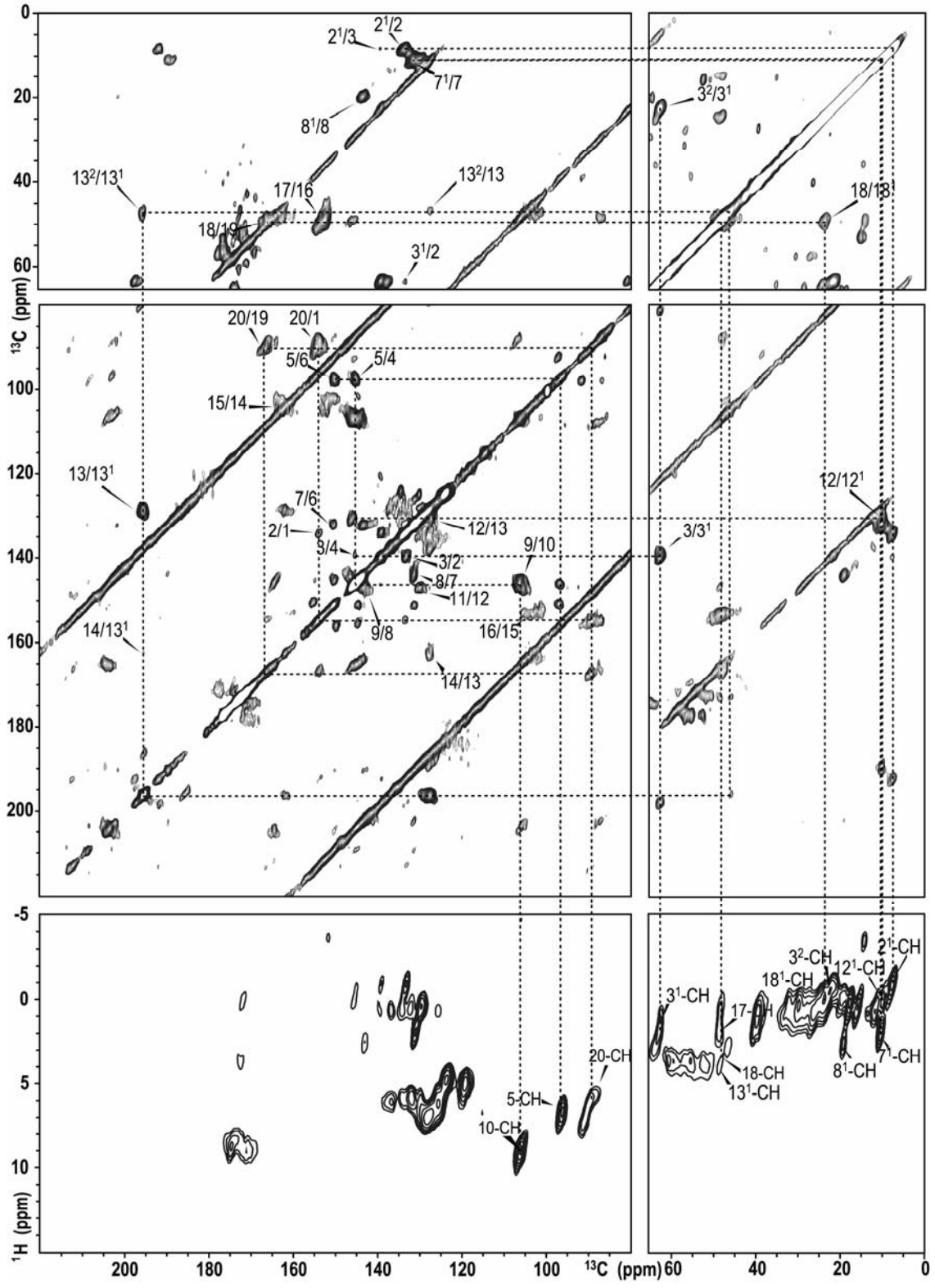

Figure 4.1 The upper panels represent contour plot sections of a ^{13}C-^{13}C MAS NMR dipolar correlation spectrum of chlorosomes isolated from the *bchQRU* mutant recorded in a field of 17.6 T using a spinning frequency of 11 kHz and a mixing time of 1.4 ms. The lower panels show contour plot sections of an ^{1}H-^{13}C MAS NMR FSLG dipolar correlation spectrum recorded in the same field employing a spinning rate of 13 kHz.

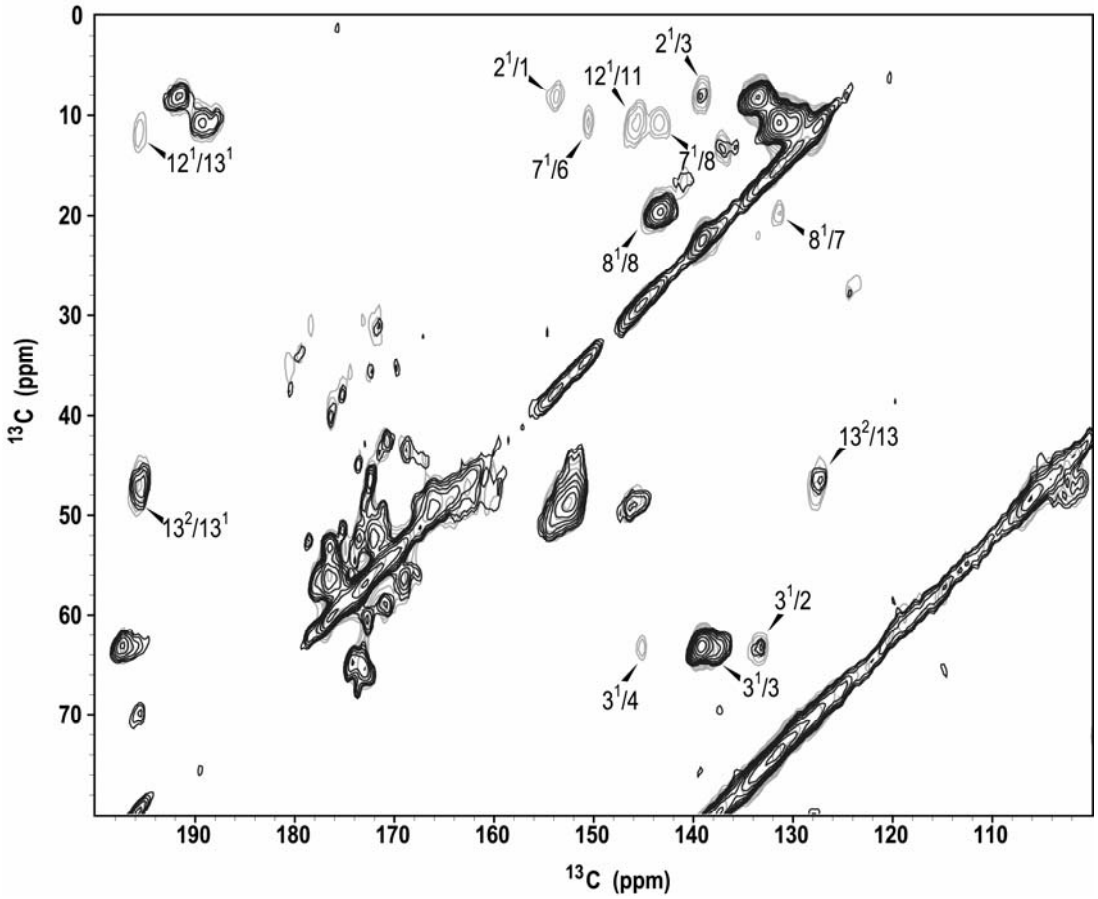

Figure 4.2 An overlay of two ^{13}C-^{13}C MAS NMR dipolar correlation spectra of the *bchQRU* mutant recorded in a field of 17.6 T using a spinning frequency of 11 kHz. The black and grey spectra were acquired at mixing times of 1.4 ms and 2.9 ms, respectively.

4.3 Results

4.3.1 Chemical shift assignment

The assignments of the ^{13}C and ^{1}H signals of the BChl *d* molecules in the *bchQRU* mutant chlorosomes were obtained from two-dimensional ^{13}C-^{13}C and ^{1}H-^{13}C dipolar correlation spectra (Figure 4.1) collected from ^{13}C-enriched chlorosomes. Relayed transfer from the 2^1, 7^1, and 12^1 carbons to their second-nearest neighbors allowed the unambiguous assignment of those methyl signals from an RFDR dataset recorded with a 2.9 ms mixing time (Figure 4.2). The 8^1 response could not be resolved from the 8^2-^{13}C signal. The assignment of the 4, 6, and 11 positions was confirmed from relayed transfer correlations also using the dataset recorded at the mixing

time of 2.9 ms. The 11- carbon can also be assigned from relayed $12^1/11$ transfer. A ^{13}C-^{13}C dataset recorded at a longer mixing time of 5.1 ms was needed to assign the farnesyl tail of BChl *d,* which meant that the tail is subject to restricted mobility. The ^{13}C and ^{1}H chemical shift assignment is given in Tables 4.1 and 4.2 respectively. The lines observed in ^{13}C-^{13}C correlation datasets were very narrow, of the order of 1 ppm. In the ^{1}H-^{13}C dataset, the responses in the range of 7 - 10 ppm on the ^{1}H scale are attributed to signals from a protein fraction in the sample. The NH protons correlate with the CO of the preceding amino acids, and resonate with a ^{13}C chemical shift of ~ 175 ppm [41].

Table 4.1 ^{13}C solution (σ_{liq}^{C}) and solid-state chemical shifts (σ_{i}^{C}) of BChl *d*, as well as aggregation shifts $\Delta\sigma_i^C = \sigma_i^C - \sigma_{liq}^C$ and calculated ring-current shifts of the *syn-anti* monomer stack $\Delta\sigma_{calc}^{C}$ in ppm.

Position	σ_{liq}^{C}	σ_{i}^{C}	$\Delta\sigma_{i}^{C}$	$\Delta\sigma_{calc}^{C}$
1	155.4	154.3	-1.1	-2.0
2	135.9	133.7	-2.2	-4.4
3	144.9	139.4	-5.5	-4.3
4	148.4	145.7	-2.7	-3.3
5	100.8	97.2	-3.6	-2.7
6	153.0	150.6	-2.4	-1.9
7	134.4	131.7	-2.7	-1.0
8	144.8	143.7	-1.1	-0.5
9	146.6	146.0	-0.6	0.2
10	108.1	106.7	-1.4	-1.3
11	147.7	146.4	-1.3	-3.3
12	133.7	130.2	-3.5	-4.2
13	131.3	127.8	-3.5	-3.4
14	162.6	162.4	-0.2	-2.4
15	105.8	104.0	-1.8	-1.3
16	155.3	152.9	-2.4	-0.7
17	51.2	48.5	-2.7	0.2
18	49.9	48.4	-1.5	0.5
19	169.4	166.5	-2.9	0.1
20	92.7	89.5	-3.2	-0.1
2^1	11.5	7.8	-3.7	-4.1
3^1	65.8	62.9	-2.9	-4.3
3^2	26.3	22.0	-4.3	-3.3
7^1	11.2	10.4	-0.8	0.4
8^1	20.1	19.4	-0.7	0.1
8^2	18.0	[a]		
12^1	12.9	10.1	-2.8	-2.8
13^1	199.1	195.9	-3.2	-2.0
13^2	49.2	47.3	-1.9	-0.9
17^1	30.5	30.0[b]	-0.5	0.5

Table 4.1 *(continued)*				
17^2	31.4	30.0[b]	-1.4	[d]
17^3	174.6	[c]		[d]
18^1	23.8	23.9	0.1	0.6
F1	62.4	[c]		[d]
F2	117.7	118.7	1.0	[d]
F3	143.4	142.1	-1.3	[d]
F4	39.2	39.3	0.1	[d]
F5	27.0	27.1	0.1	[d]
F6	123.4	123.9	0.5	[d]
F7	136.3	135.3	-1.0	[d]
F8	39.5	39.7	0.2	[d]
F9	27.6	27.4	-0.2	[d]
F10	123.9	124.5	0.6	[d]
F11	132.1	130.9	-1.2	[d]
F12	25.1	25.7	0.6	[d]
F3′	15.8	16.8	1.0	[d]
F7′	10.8	13.4	2.6	[d]
F11′	17.0	[c]		[d]

[a] The 8^2 response could not be resolved from the 8^1 signal. [b] The signals for 17^1 and 17^2 are overlapping in the spectra. [c] Signals for 17^3, F1, and F11′ could not be resolved. [d] Farnesyl tail was replaced by CH_3 at 17 for ring-current shift calculation.

Table 4.2 ^{1}H solution (σ_{liq}^H) and solid-state chemical shifts (σ_i^H) of BChl *d*, as well as aggregation shifts $\Delta\sigma_i^H = \sigma_i^H - \sigma_{liq}^H$ and calculated ring current shifts $\Delta\sigma_{calc}^H$ for the four models in ppm.

Position	σ_{liq}^H	σ_i^H	$\Delta\sigma_i^H$	$\Delta\sigma_{calc}^H$			
				A	B	C	D
5	8.6	6.6	-2.0	-2.4	-7.4	-4.3	-2.9
10	8.6	9.0	0.4	-0.8	-0.8	+1.3	-1.1
17	3.3	1.9	-1.4	-0.1	-1.0	-0.1	0.3
18	3.6	3.4	-0.2	-0.9	-0.6	-0.5	0.7
20	7.4	6.2	-1.2	-1.1	-0.9	-4.2	-0.4
2^1	2.4	-0.9	-3.3	-1.9	-3.0	-7.6	-4.0
3^1	5.4	1.7	-3.7	-2.9	-10.6	-5.2	-3.0
3^2	1.2	-0.4	-1.6	-3.2	-7.0	-7.8	-3.2
7^1	2.4	2.0	-0.4	1.0	-2.0	0.3	0.4
8^1	2.9	2.6	-0.3	1.0	-0.3	1.0	0.1
8^2	0.8	[a]					
12^1	2.7	0.1	-2.6	-2.5	-0.8	1.1	-2.4
13^2	4.3	4	-0.3	-2.0	-3.1	0.9	-0.5
17^1	1.4/1.7	[a]		-0.3	-0.3	0.4	0.6
17^2	1.3/1.7	[a]			-0.1	0.0	
18^1	1.0	0.0	-1.0	-0.1	-1.1	-0.8	0.7

A: Parallel-stack model [18]; B: Piggy-back dimer model [42]; C: Antiparallel monomer stack model (this study); D: *Syn-anti* monomer stack model (this study); [a] Correlation peaks are not resolved.

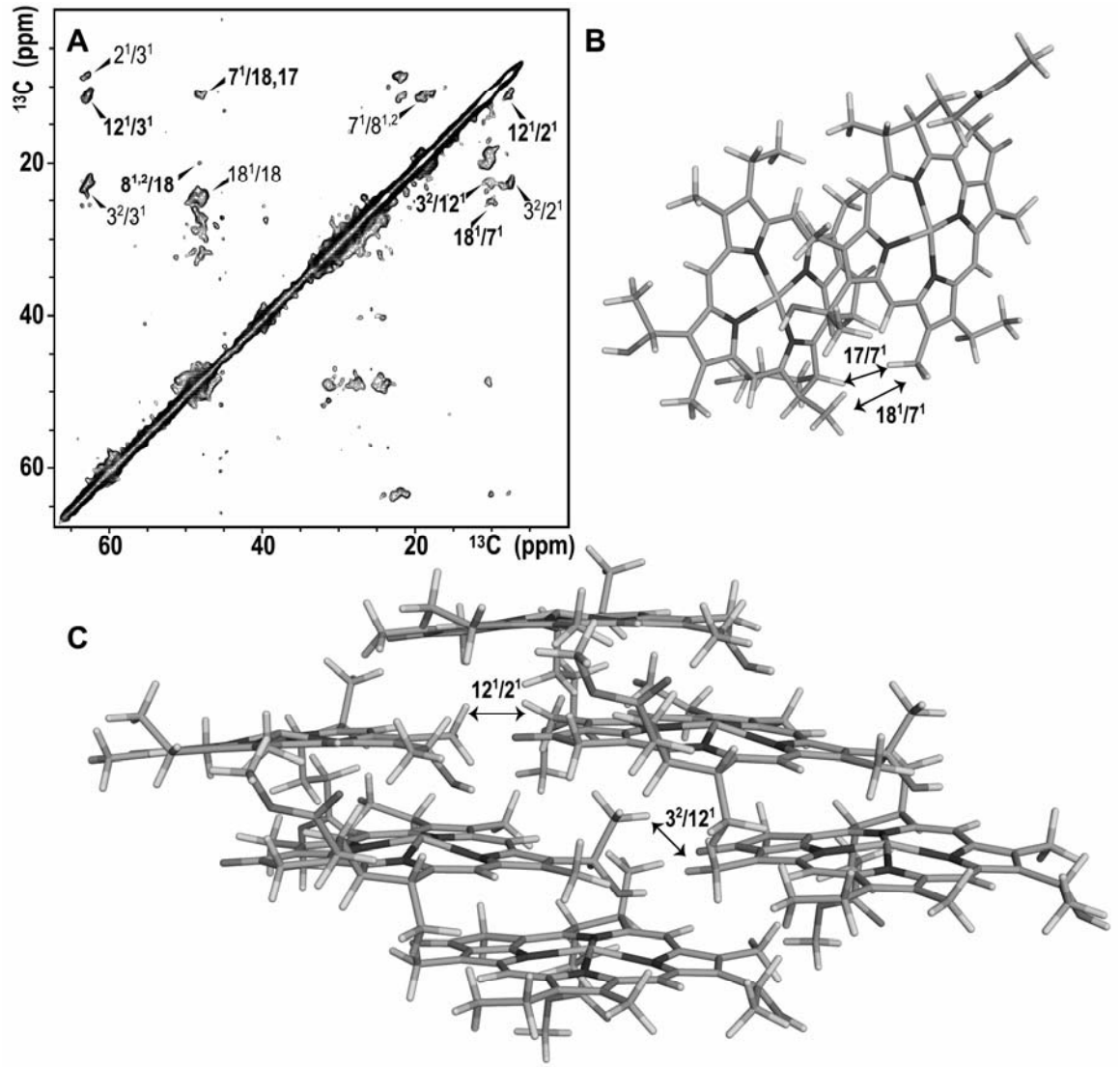

Figure 4.3 (A) ^{13}C-^{13}C CHHC dataset of *bchQRU* chlorosomes, recorded at 17.6 T with 13 kHz spinning and 250 μs spin diffusion. Correlations labeled in bold and normal type face, respectively, are intermolecular and intramolecular. (B) Two BChl *d* molecules (farnesyl tails are replaced by methyl groups) in a single *syn-anti* unit. The arrows indicate the side chains between which cross-peaks are seen. (C) Two stacks with inter-stack cross-peaks indicated.

4.3.2 Distance constraints

To proceed from an assignment to the structure, we used the CHHC experiment with a short mixing time of 250 μs [28]. Intermolecular correlations between BChl *d* molecules within a chlorosome were detected (highlighted in bold type face in Figure 4.3A) that led us to identify a new, alternating stacking mode for the basic unit in the suprastructure. Since

no intramolecular pathway that could serve to correlate the resonances over a 250 μs mixing time exists in the proton network, these correlations could be assigned unambiguously. The $7^1/18$, and $7^1/18^1$ intermolecular contacts observed were especially significant because very few possibilities for molecular assembly exist in which these atoms are in close proximity.

They revealed the presence of alternating monomers forming stacks assembled into layers with the farnesyl tails alternately extending on both sides. We found two possible intermolecular arrangements that can satisfy these constraints: a stack built from alternating *syn* and *anti* monomers (Figure 4.3C) or antiparallel monomer stacking (Figure 4.5C). The *syn-anti* monomer stack has alternating molecular conformations of the C-3 side chain, and *syn* or *anti* refers to the orientation of the OH ligation of adjacent BChls with respect to the farnesyl side chain. The intermolecular contacts corresponding to a single *syn-anti* unit from the stack are shown in Figure 4.3B. Intermolecular correlations between carbons $12^1/3^1$, $12^1/2^1$, and $12^1/3^2$ were detected between rings I and III of two BChl *d* molecules from adjacent stacks (Figure 4.3C).

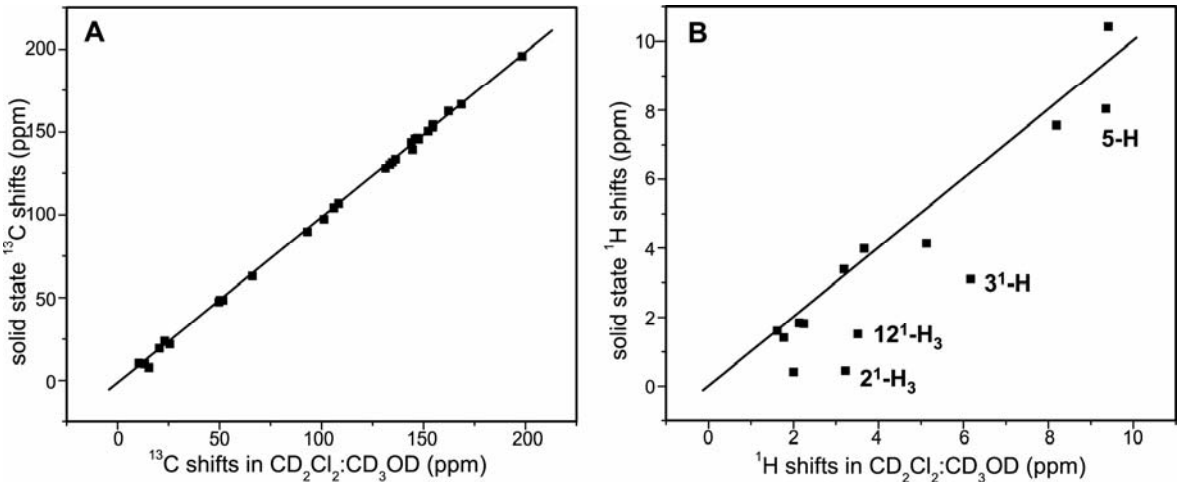

Figure 4.4 Chemical shift correlation plots of *bchQRU* chlorosomes. The ^{13}C and ^1H shifts in the solid sample are plotted against the monomer shifts in a CD_2Cl_2 solution with 5% CD_3OD. The solid lines represent the diagonals. ^1H signals are indicated that show a large upfield shift in the solid relative to the monomer.

4.3.3 Aggregation and ring-current shifts

Figure 4.4 compares the ^{1}H and ^{13}C chemical shifts for the *bchQRU* chlorosomes with the corresponding monomer shifts in solution. These correlation plots clearly show how pronounced the ^{1}H aggregation shifts are within the ^{1}H chemical shift range, in contrast to the ^{13}C aggregation shifts. The ^{1}H aggregation shifts are dominated by ring-current effects, in line with observations in other chlorophyll aggregates, and are more useful than the ^{13}C shifts for structure determination [43]. Significant observed upfield ^{1}H aggregation shifts ($\Delta\sigma_i^H$) for the *bchQRU* chlorosomes are displayed as circles in Figure 4.6 for values less than -1.5 and -2.5 ppm respectively.

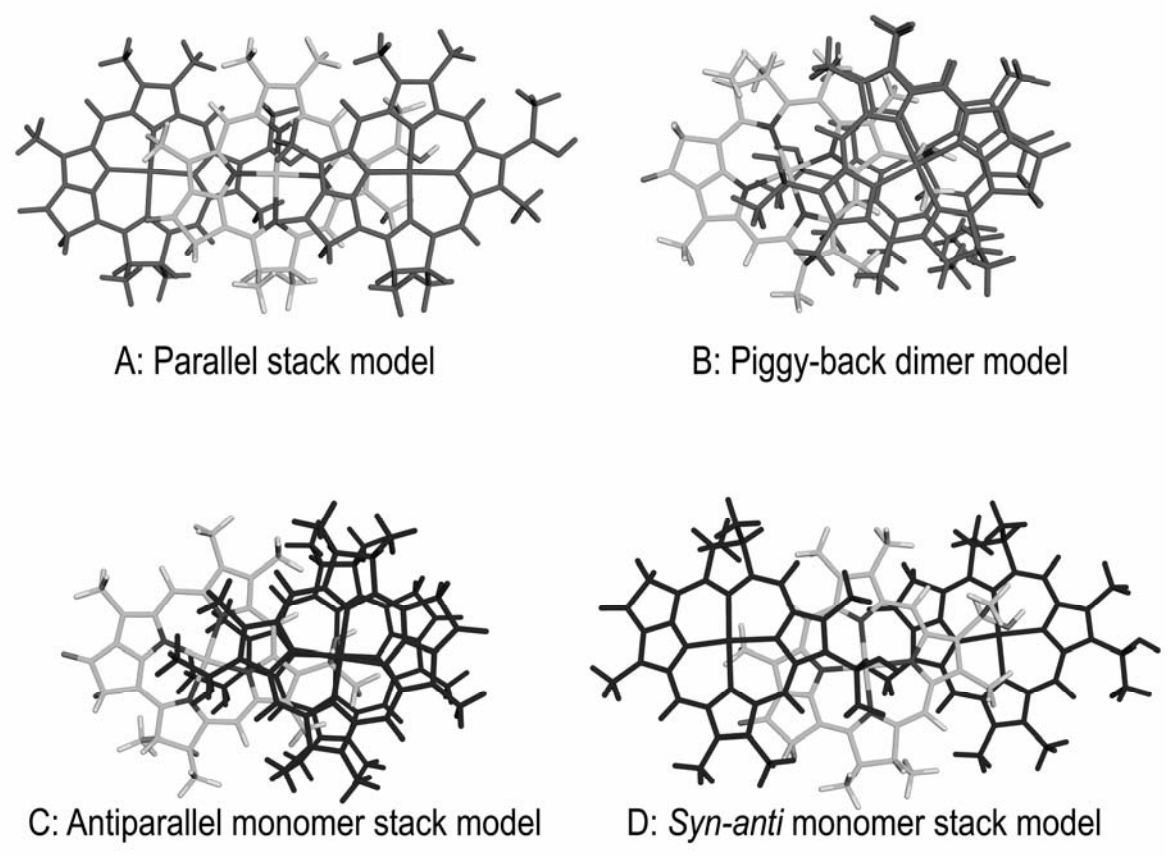

Figure 4.5 The four models used in the ring-current shift calculations. The BChl *d* rings denoted in black are the major contributors to the ring-current effects on the BChl *d* ring system shown in grey and are explicitly used in the calculation. To simplify the calculations, the ethyl group at C-8 and the propionate side chain with its attached farnesyl tail at C-17 were substituted by methyl groups.

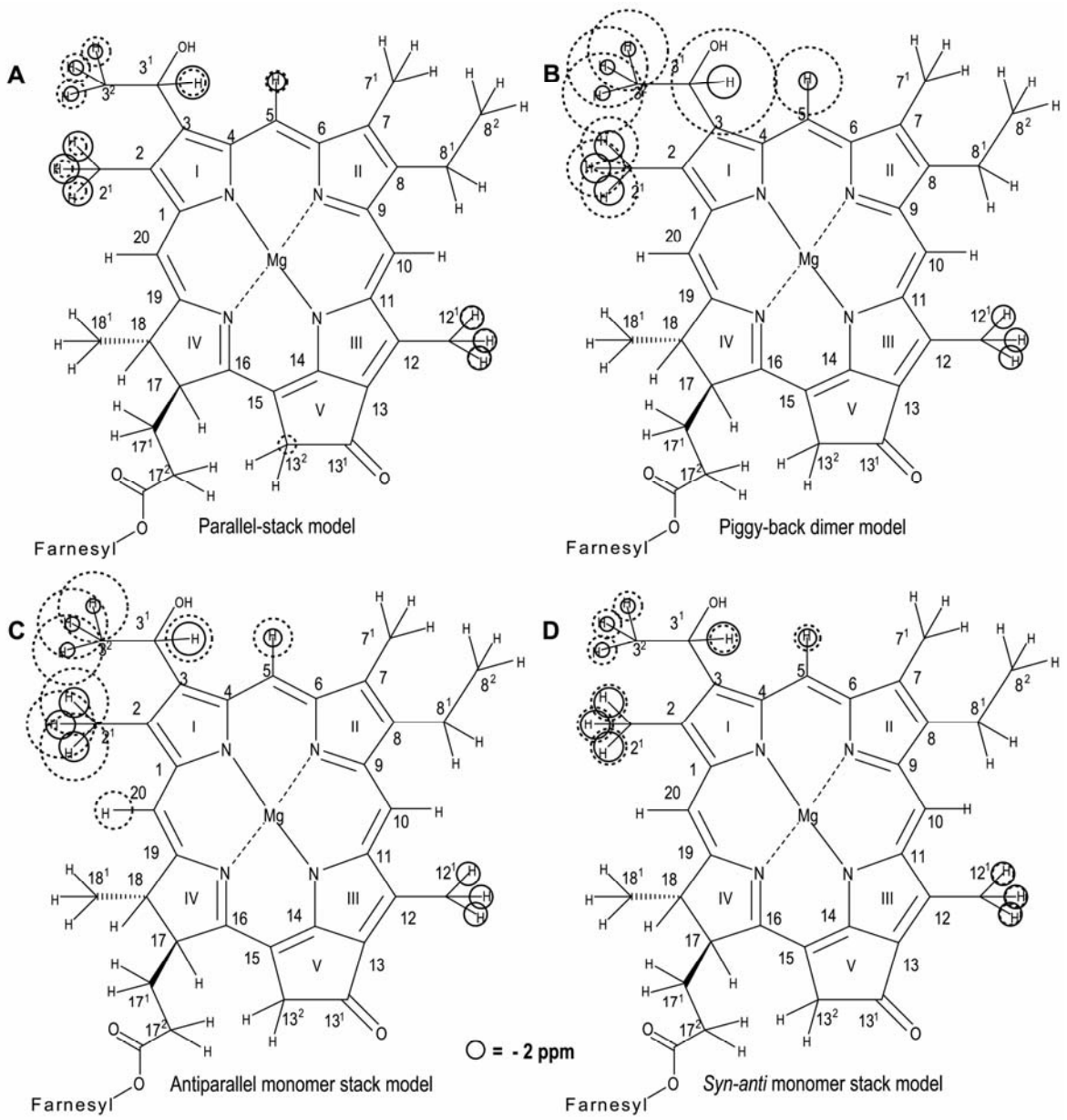

Figure 4.6 The observed ^{1}H upfield aggregation shifts of the *bchQRU* chlorosomes relative to the monomer in solution are shown as dark circles for values less than -1.5 ppm. The calculated ring-current shifts for the (A) Parallel-stack model, (B) Piggy-back dimer model, (C) Antiparallel monomer stack model, and (D) *Syn-anti* monomer stack model are represented by the dashed circles. The circles have a radius proportional to the magnitude of the shift.

Table 4.2 lists the calculated ^{1}H ring-current shifts for the parallel-stack (A), the piggy-back dimer (B), the antiparallel monomer stack (this study) (C), and the *syn-anti* monomer stack (this study) (D) [18,42]. The

molecular arrangements used for the ring current shift calculations are depicted in Figure 4.5, which shows the overlap for adjacent molecules in the structure. The ring-currents $\Delta\sigma^{H}_{calc}$ and $\Delta\sigma^{C}_{calc}$ were calculated for each proton and carbon that resides within the shielding area of adjacent overlapping BChl *d* molecules.

These calculations showed that only the *syn-anti* monomer stack and the parallel-stack reproduced the experimental ring-current shifts that are observed. In these two arrangements, each BChl molecule has significant overlap with two adjacent molecules, over ring I and over ring III, at opposite sides of the BChl. Since the parallel-stack violated the NMR distance constraints, there was converging and convincing evidence for a structure built from *syn-anti* monomer stacks. The calculations for the piggy-back dimer model gave anomalously large proton ring-current shifts at 5-H, 3^1-H, and 3^2-H_3, while the anti-parallel monomer stack gave a mismatch over the entire overlap region of 1-5 and 15-13^2. In these two arrangements there is pronounced overlap with two neighbors at ring I, with correspondingly large ring current shifts, and little overlap at ring III, and this leads to the asymmetry in the ring current shift patterns (Figure 4.6). However, no such asymmetry was observed in the experimental data.

4.3.4 Cryo-EM data

In end-on views of *bchQRU* mutant chlorosomes, the BChls can be observed to form coaxial cylinders or tubes (Figure 4.7B). In side views of chlorosomes, the concentric layers that form the chlorosome nanotubes produce a regular pattern with a spacing of 2.1 nm (Figures 4.7A and D) [22,23]. Additionally, a distinct striped pattern with a spacing of 0.83 ± 0.01 nm is seen, at a 90°-angle to the layers (Figures 4.7C and D). After Fourier transformation the layers translated into a single pair of equatorial reflections while the stripes gave rise to layer lines that are characteristic of a helical arrangement with an axial repeat of 0.83 nm, corresponding to the separation between the BChl *d* stacks. Figures 4.7E and G show a model of four coaxial tubes that is consistent with all data obtained.

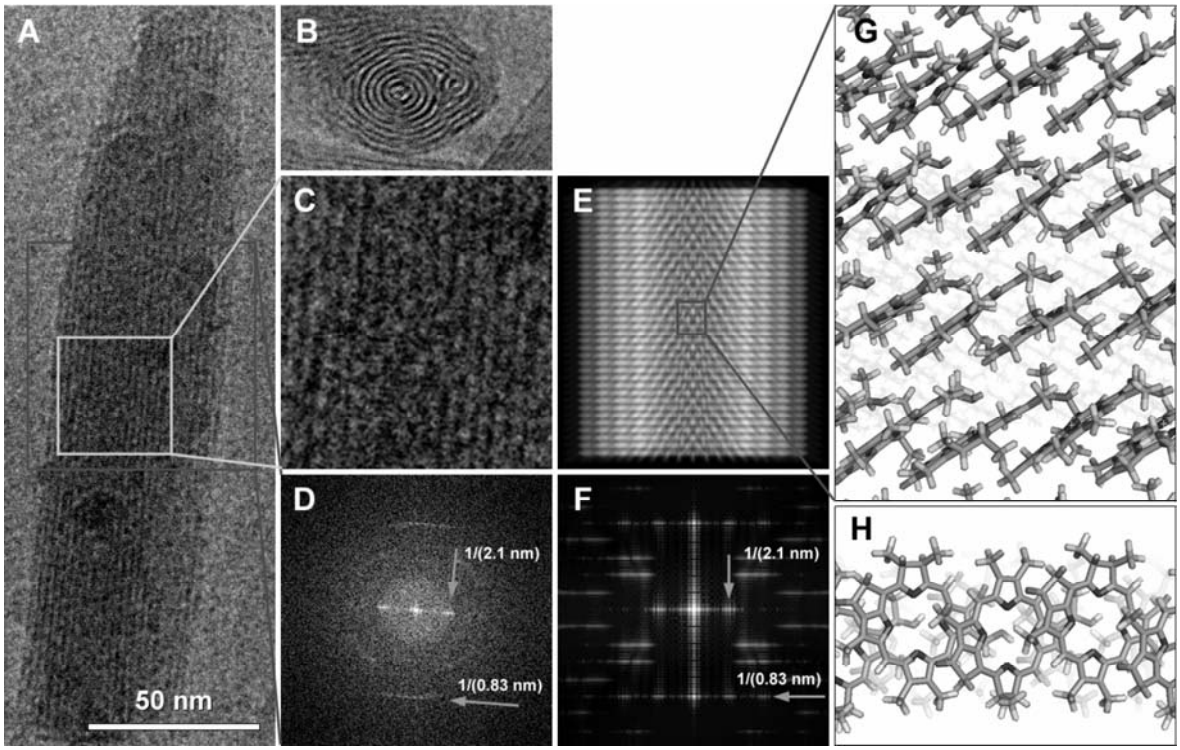

Figure 4.7 Cryo-EM images of isolated chlorosomes from the *bchQRU* triple mutant of *C. tepidum* embedded in amorphous ice (Panels A and B). A chlorosome is seen in side-on view in Panel A and in end-on view, showing the involuted layering of the BChls, in Panel B. Panel C shows an enlarged region of the side-on view, indicated by the grey box in Panel A. Panel D shows the fourier transform of the black-boxed region in Panel A. The grey arrows indicate reflections from a 2.1-nm spacing between BChl layers and a 0.83-nm spacing along the layers. Panels E and F depict simulated EM image and its Fourier transform, from a 17^2-farnesyl-*R*-[E,M] BChl *d* helical rod model comprising 4 tubes with the BChl stacks running perpendicular to the tube axis. G. Enlarged view of the boxed area in E. H. Top view, *i.e.* along the tube axis.

4.4 Discussion

4.4.1 NMR and cryo-EM in tandem for the suprastructure

The 17^2-farnesyl-*R*-[E,M] BChl *d* produced by the *bchQRU* mutant led to a well-defined, extended chlorosome structure. The 0.83-nm periodicity in *bchQRU* chlorosomes corresponds to the spacing between adjacent, NMR derived and geometry optimized *syn-anti* monomer stacks that run along the circumference of a tube, perpendicular to the axis. A stack is defined as the structure for which one goes from one molecule of BChl to the next

one via the O-Mg coordinate bond, then in the same molecule from the OH group again to the Mg of the next BChl molecule. In contrast, the optical transition dipole moment for the monomer runs through the C-13^1 carbonyl group, along the hydrogen bonds. After excitation, the excitons move through the BChl aggregates along helical trajectories following the O—H···O=C connection pathway that reflects the macroscopic chirality of the system [44].

To arrive at a model for the arrangement of BChls in the chlorosomes of the *bchQRU* mutant forming a multi-layer tubular structure, supramolecular models were built for different orientations of the stacks relative to the tube axis. First, a larger section of the *syn-anti* structure comprising six stacks with twelve BChl *d* molecules each was optimized using molecular mechanics. A *syn-anti* unit taken from this optimized structure was used to construct the larger single-and multi-layer tubular structures. From these atomic models the electron density was calculated and projected down to create side-views at a resolution of 0.6 nm for comparison with the experimental cryo-EM data.

There are many different ways to organize the stacks together to form a cylinder. One extreme is with the stacks running parallel to the tube axis, and the other extreme has the stacks running along the circumference of the tube, perpendicular to the tube axis (Figures 4.7 and 4.8). For stacks running parallel to the tube axis, the BChl monomers connected via the hydrogen bond to the carbonyl of the BChl in the adjacent stack to form a left-handed helix while for stacks running perpendicular to the tube axis the helicity of the H-bonded sequences form right-handed helices. When tubes are formed by bending the molecular arrays in the opposite direction, the helicities change sign. This partially explains why the circular dichroism response of chlorosomes strongly depends on the sample preparation [45]. In addition it is also known that the circular dichroism spectra depend strongly on the aggregate length of the chlorosome [44].

For stacks running perpendicular to the tube axis, along the circumference of a cylinder, the simulated image and its Fourier transform reproduced the strong periodicity of 0.83 nm and the distinct striped

appearance that was seen in images of the *bchQRU* mutant chlorosomes (Figure 4.7). The 2.1 nm spacing is reproduced by combining several coaxial cylinders with an increment in the radius of 2.1 nm (Figure 4.7E and F). The inclination of the optical transition dipole moment with respect to the long axis of the tube is ~55 degrees. This indicates that in the chlorosomes of the *bchQRU* mutant, the stacks run at an angle of ~90 degrees to the tube axis. The high contrast of the structure in the chlorosomes of the *bchQRU* mutant presumably arises from the orientation of the BChl molecules: the plane of the molecules being along the optical axis, the projection direction of the microscope, and the direction of the stacks, along the circumference of the tubes, which creates a strong alternation of high and low projected scattering density along the tube axis direction.

A suprastructure framework according to Figures 4.7 and 4.8 allows for structural variability. In particular, rotation of the stacks relative to the tube axis produces periodicities between 0.83 and 1.25 nm. While rotated stacks failed to reproduce the characteristic appearance of the *bchQRU* mutant chlorosomes, for stacks of dimers running parallel to the tube axis the Fourier transform of the projected model structure shows a layer line at 1/1.25 nm^{-1}. This periodicity corresponds to the distance between the repeating *syn-anti* pairs in the direction of the stacks (Figure 4.8). For WT chlorosomes no distinct spacing, similar to that in *bchQRU* mutant chlorosomes, could be detected visually in the cryo-EM images. However, Fourier transforms of the images clearly showed the presence of a layerline at 1.22 ± 0.03 nm^{-1} (Figure 4.9). The monomer transition moments and the inclination of the transition dipole with respect to the long axis of the tube are ~36 degrees as seen for the chlorosomes of *Cf. aurantiacus* [44].

Although the WT chlorosomes are much more heterogeneous than the chlorosomes from the *bchQRU* mutant and contain BChl *c* molecules with variable degrees of methylation at carbons C-8^2 and C-12^1 and both *R*- and *S*- chirality at carbon C-3^1 that has prevented thus far a precise determination of the structure at the molecular level our data suggested that an overall dimeric character at the basis is present in the WT, with

stacks running parallel to the tube axis. Interestingly, the two supramolecular arrangements with stacks running parallel or perpendicular to the tube axis allow for similar O—H···O=C connection pathways (Figure 4.8).

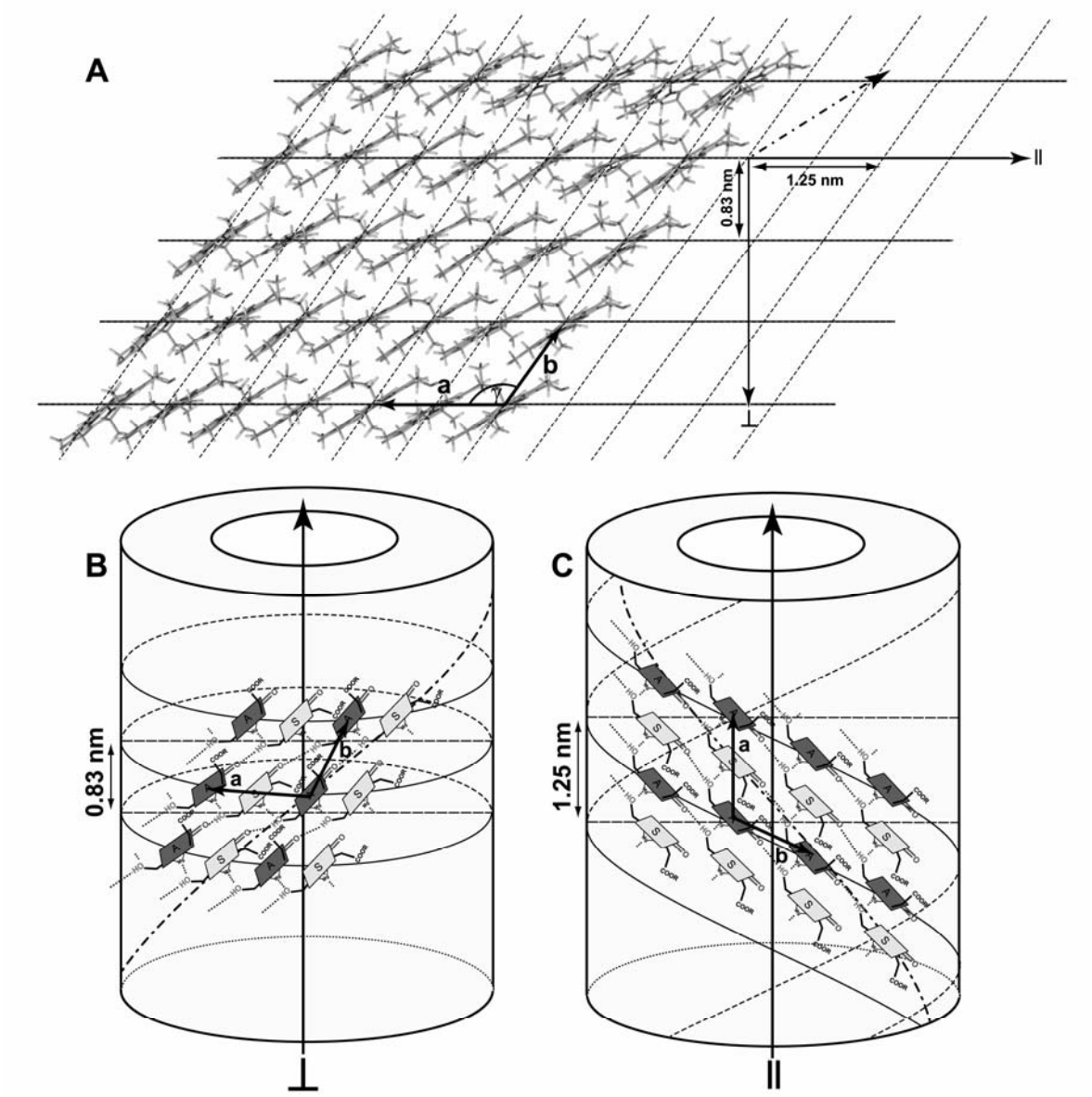

Figure 4.8 (A) 7×5 section of the *syn-anti* array. The stacks are separated by 0.83 nm and the unit cell dimensions are: a = 1.25, b = 0.98, γ = 122°. The repeat along the stack is 1.25 nm. (B) and (C) Schematic tube models with stacks running perpendicular or parallel to the tube axis. Periodicities of 1.25 nm and 0.83 nm are indicated. The H-bond helix that supports the exciton delocalization is shown with dotted-dashed lines. Rotation of the stacks relative to the tube axis produces periodicities between 0.83 and 1.25 nm.

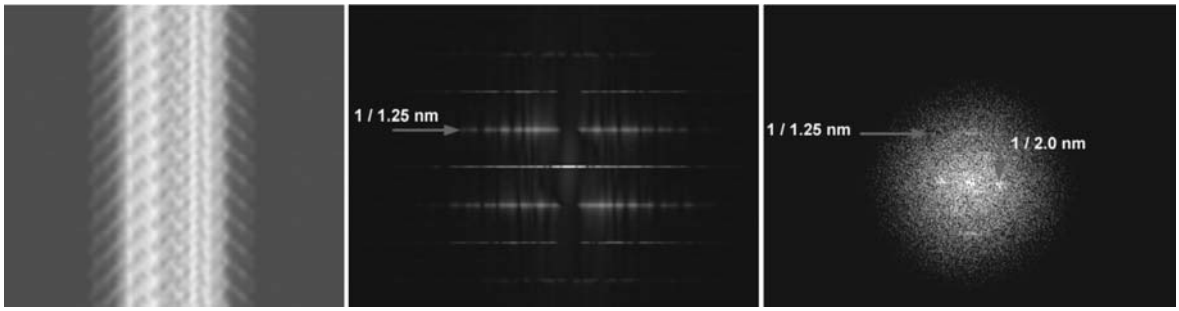

Figure 4.9 From left to right: the simulated image of a single tube with stacks of dimers running parallel to the tube axis, the Fourier transform of the tube in the middle panel, and the Fourier transform of an experimental cryo-EM image of a WT chlorosome in the right panel.

In the molecular modeling the two configurations having stacks running parallel or perpendicular to the tube axis correspond with local minima in the energy landscape of the suprastructure that permits the embedding of chemical heterogeneity. For instance, methylation in the WT is used to tune the exact wavelength of the Q_y absorption maximum and to increase the absorption cross-section by inhomogeneous broadening due to the many different microenvironments of the BChl *c* mixture [14]. However, in the *bchQRU* mutant this microheterogeneity does not exist. With only 17^2-farnesyl-*R*-[E,M] BChl *d* the absorption spectrum is much narrower and shifts to the blue by ~15 nm [24]. The suprastructure with stacks running parallel to the tube axis must be sufficiently stable to accept BChl *c* with methyl or ethyl side chains at C-12 and ethyl, propyl, or isobutyl side chains at C-8. Likewise, the suprastructure must accommodate the variable amounts of BChls with *R* and *S* chirality that the WT organism normally produces. Based on the modeling it cannot be excluded that the direction of the BChl stacks deviates slightly from the two models for WT and *bchQRU* mutant presented here. The expected spacing in the direction of the tube is not sensitive to small variations around the 0 and 90 degree orientation of the stacks. Stacks forming shallow left- or right-handed helices in *bchQRU* chlorosomes and stacks forming steep helices and WT chlorosomes would still be consistent with the experimental EM data.

4.4.2 Suprastructure heterogeneity in chlorosomes

The structural features of the chlorosome, both at the molecular level, and at the level of the suprastructure: *i.e.*, whether the structure formed by the BChl aggregates was rod-like or lamellar, have been an important and controversial issue in the biophysics and photosynthesis communities for more than two decades [23,46]. Cryo-EM and diffraction experiments agree in that they always produce essentially the same spacing for the BChl layers [22,23]. The spacing between layers for the chlorosomes of the *bchQRU* mutant is 2.10 ± 0.12 nm (Figure 4.7). This matches the layer separation of 2.1 nm observed in the WT chlorosomes (Figure 4.9) [22]. Chlorosomes of mutants lacking all carotenoids also have the same BChl sheet spacing, about 2.1 nm, as those containing normal levels carotenoids [47]. Apparently, the self-organization into a single layer is a common property that is preserved across a variety of species [22]. It provides an important constraint on the microstructure.

The predominant 17^2-farnesyl-*R*-[E,M] BChl *d* in the chlorosomes of the *bchQRU* mutant leads to a much better organized and homogeneously ordered structure than the heterogeneous BChl *c* mixture in WT chlorosomes. In addition to the stacking direction, the curvature of the tubes, as well as the number and types of tubes, apparently correlates with and likely arises from the degree of chemical heterogeneity of the samples. In the *bchQRU* mutant there are clearly longer tubes (*z*-axis, parallel to the membrane plane) and fewer tubes per chlorosome than for the WT [48]. In contrast, in the majority of the mutant chlorosomes, there are only one or two nanorods, the extreme with the lowest possible edge fraction.

These observed differences probably have biological significance. As measured by the growth rate of cells, the much larger WT chlorosomes actually outperform the chlorosomes of the *bchQRU* mutants at all light intensities between 5 and 200 µmol photons m^{-2} s^{-1} [14]. When grown at very low light intensity (~5 µmol photons m^{-2} s^{-1}), *C. tepidum* cells produce about three times more BChl *c* than cells grown at high light intensity (>100 µmol photons m^{-2} s^{-1}), but since the cell size does not change and the number of chlorosomes per cell does not change dramatically, the

number of BChls per chlorosome must increase by about 3-fold [14]. Consistent with the idea that the BChls reside in a larger number of environments, the half-band width of the Q_y absorption maximum of the BChl *c* aggregates is largest for WT chlorosomes isolated from cells grown at low light intensity and is also much broader than for chlorosomes of the *bchQRU* mutant [14]. *C. tepidum* synthesizes a higher proportion of BChls with *S*-chirality at C-3^1 at low light intensity, and this may produce a larger number of "BChl domains" per chlorosome as well as smaller "domains" as marked by edges [49]. Thus, the organism avoids producing arrays with larger and larger numbers of BChl *c* at decreasing light intensity. A very large increase in the domain size of the antenna would probably reduce the energy transfer efficiency to the baseplate BChl *a* (B_{790}), the BChl *a*-binding Fenna-Matthews-Olson protein, and ultimately the reaction centers. For instance, methylation in the WT is used to tune the exact wavelength of the Q_y absorption maximum and to increase the absorption cross-section by inhomogeneous broadening due to the many different microenvironments of the BChls [14]. However, in the *bchQRU* mutant this microheterogeneity does not exist. Without the modified side chains at C-8 and C-12, which in the mutant are only ethyl and methyl groups, respectively, the absorption spectrum is much narrower and shifts to the blue by ~15 nm [24].

4.4.3 The mechanism of self-assembly of BChl d

From modeling it was proposed that the self-assembly is driven by non-covalent interactions without requiring proteins for structural control [18,50]. These interactions are coordination of the C-3^1-hydroxyl to the magnesium ion, hydrogen bonding between the C-3^1-hydroxyl to the C-13^1-keto group, π-π stacking between the extended chlorin chromophores and partitioning of aliphatic tails into the hydrophobic part of the suprastructure. The embedding of chemical heterogeneity in the suprastructure produces interactions at the molecular level competing with packing effects that result from the stiffness of the suprastructure [51]. In this way an asymmetry at the molecular level can propagate to have a strong impact on the suprastructure. In a stack built from

alternating *syn* and *anti* conformers with pure (*R*) chirality, the out-of-plane rotation of the C-3 side chain alternates between adjacent monomers in the stacks. A BChl layer built only from *R*-stereoisomers arranged in *syn-anti* units has a tendency to bend when modeled in a molecular mechanics energy minimization procedure, which extrapolates into rings and rods. *S* chirality admixture relaxes the strain, if *R*- and *S*-BChls occupy alternating positions in the stack. Hence, a predominant (*R*) fraction in a *syn-anti* monomer packing scheme can help to support an involuted suprastructure, which is in agreement with the rods that are observed by cryo-EM of the chlorosomes (Figure 4.7). The molecular strain involved is weak, as the curvature can easily be changed to generate concentric tubes with different radii, and it does not give rise to a pronounced difference of the NMR signals from the *syn* and *anti* conformers, due to the pseudo-symmetry of the *syn-anti* building block.

With pure *R*-BChls in antiparallel monomer stacks, however, the same arguments above apply but in the opposite direction. *A priori,* there is no additional mechanism for symmetry breaking from the C-3 functionality, since the antiparallel monomer stack flips the BChl molecules around in such a way that there is no need to rotate the C-3 side chain. In Chapter 6 the NMR structure of Zn-chlorin model systems has been studied, which lack chirality at the C-3 position, and as inferred from the NMR studies of these systems, they produce planar structures with a pattern of strong ring-current shifts that is reproduced well by the DFT calculations for the antiparallel monomer stacking in Table 4.2 [52]. In order to accommodate an *S*-epimer in an antiparallel stack built from *R*-BChl epimers, the C-3 side chain must be flipped over, and symmetry breaking is established that can lead to physical frustration and stabilization of curvature. The greater the proportion of *S*-epimers, the more strain is introduced into the system, until at *R:S* = 1:1, a maximum is reached. Hence, in contrast to the *syn-anti* monomer stack model, strong mixed chirality is needed for antiparallel monomer stacking to achieve more pronounced curvature, while a pure stereoisomer favors planarity and produces a lamellar suprastructure, in contrast with the EM observations.

A difference in concentration between *R*- and *S*- epimers, or a deviation from purity, thus represents symmetry breaking, but to achieve this, different packing modes are required. BChls with *S*-chirality are never more than about 10% of the total BChl *in vivo* [49]. It is highly unlikely that the amount of *S*-chirality in the BChls of the *bchQRU* mutant would be larger than for WT. In WT *C. tepidum*, the proportion of *S*-chirality in BChl homologs increases as methylation at C-8^2 and C-12^1 increase, which in turn increase at low light intensity; however, in the *bchQRU* mutant, no methylation at all occurs at C-8^2 and C-12^1 and the organism is actually unable to adjust the cellular content of BChl [24]. As a result, the amount of *S*-BChl *d* in the mutant is expected to be lower than in the WT, on the order of 5% of the total BChl.

4.5 Conclusions

For a member of the class of chlorosome antennae, from the *bchQRU* mutant of *C. tepidum*, a genetic construct that produces only [E,M]-BChl *d* with predominantly the *R*-stereoisomer at C-3^1, we have determined a highly defined nanotubular suprastructure comprising of coaxial monolayer tubes that are assembled from a basic unit consisting of two conformers, *syn* and *anti*. The occurrence of a single BChl *d* homolog with reduced *S*-chirality for chlorosomes from the *bchQRU* mutant correlates with much larger BChl domains and fewer nanotubes per chlorosome. The mutant suprastructure is built from stacks that consist of alternating *syn-anti* BChl *d* molecules. The stacks form rings perpendicular to the tube axis that self-assemble into coaxial cylinders to form nanotubes. The structure in chlorosomes of the *bchQRU* mutant is well ordered and has little variability in the monomeric building blocks. The suprastructure found in WT chlorosomes is built from dimeric stacks parallel to the tube axis. The chemical heterogeneity is embedded in the suprastructure and produces moderate disorder. This disorder from heterogeneity at the microscopic level is used to produce functional advantages, since the electronic properties of the molecules and the absorption cross-section of the antenna can easily be modified.

References

[1] N. U. Frigaard and D. A. Bryant (**2006**) *Chlorosomes: Antenna Organelles in Photosynthetic Green Bacteria*, (J.M. Shively, Eds.) Springer-Verlag, Berlin.

[2] D. A. Bryant, A. M. G. Costas, J. A. Maresca, A. G. M. Chew, C. G. Klatt, M. M. Bateson, L. J. Tallon, J. Hostetler, W. C. Nelson, J. F. Heidelberg and D. M. Ward (**2007**) *Science* 317: 523-526.

[3] J. M. Olson (**1998**) *Photochemistry and Photobiology* 67: 61-75.

[4] N. U. Frigaard, H. Li, K. J. Milks and D. A. Bryant (**2004**) *Journal of Bacteriology* 186: 646-653.

[5] V. I. Prokhorenko, A. R. Holzwarth, M. G. Muller, K. Schaffner, T. Miyatake and H. Tamiaki (**2002**) *Journal of Physical Chemistry B* 106: 5761-5768.

[6] H. Kim, H. Li, J. A. Maresca, D. A. Bryant and S. Savikhin (**2007**) *Biophysical Journal* 93: 192-201.

[7] J. Overmann, H. Cypionka and N. Pfennig (**1992**) *Limnology and Oceanography* 37: 150-155.

[8] J. T. Beatty, J. Overmann, M. T. Lince, A. K. Manske, A. S. Lang, R. E. Blankenship, C. L. Van Dover, T. A. Martinson and F. G. Plumley (**2005**) *Proceedings of the National Academy of Sciences of the United States of America* 102: 9306-9310.

[9] A. K. Manske, J. Glaeser, M. A. M. Kuypers and J. Overmann (**2005**) *Applied and Environmental Microbiology* 71: 8049-8060.

[10] A. R. Holzwarth, M. G. Müller and K. Griebenow (**1990**) *Journal of Photochemistry and Photobiology B-Biology* 5: 457-465.

[11] H. Tamiaki, A. R. Holzwarth and K. Schaffner (**1992**) *Journal of Photochemistry and Photobiology B-Biology* 15: 355-360.

[12] A. Schenning and E. W. Meijer (**2005**) *Chemical Communications*: 3245-3258.

[13] V. Huber, M. Lysetska and F. Würthner (**2007**) *Small* 3: 1007-1014.

[14] A. Gomez Maqueo Chew, N. U. Frigaard and D. A. Bryant (**2007**) *Journal of Bacteriology* 189: 6176-6184.

[15] T. Nozawa, K. Ohtomo, M. Suzuki, H. Nakagawa, Y. Shikama, H. Konami and Z. Y. Wang (**1994**) *Photosynthesis Research* 41: 211-223.

[16] T. S. Balaban, A. R. Holzwarth, K. Schaffner, G. J. Boender and H. J. M. de Groot (**1995**) *Biochemistry* 34: 15259-15266.

[17] B. J. van Rossum, D. B. Steensgaard, F. M. Mulder, G. J. Boender, K. Schaffner, A. R. Holzwarth and H. J. M. de Groot (**2001**) *Biochemistry* 40: 1587-1595.

[18] A. R. Holzwarth and K. Schaffner (**1994**) *Photosynthesis Research* 41: 225-233.

[19] J. Chiefari, K. Griebenow, N. Griebenow, T. S. Balaban, A. R. Holzwarth and K. Schaffner (**1995**) *Journal of Physical Chemistry* 99: 1357-1365.

[20] A. Gomez Maqueo Chew and D. A. Bryant (**2007**) *Annual Review of Microbiology* 61: 113-129.

[21] S. Ganapathy, M. Reus, A. G. M. Chew, D. A. Bryant, A. R. Holzwarth and H. J. M. de Groot (**2007**) in: *Photosynthesis. Energy of Sun: 14th International Congress on Photosynthesis Research*: pp. 251-254 (J.F. Allen, Ed.) Springer, Glasgow.

[22] G. T. Oostergetel, M. Reus, A. G. M. Chew, D. A. Bryant, E. Boekema and A. R. Holzwarth (**2007**) *FEBS Letters* 581: 5435-5439.

[23] J. Psencik, T. P. Ikonen, P. Laurinmaki, M. C. Merckel, S. J. Butcher, R. E. Serimaa and R. Tuma (**2004**) *Biophysical Journal* 87: 1165-1172.

[24] A. G. M. Chew, N. U. Frigaard and D. A. Bryant (**2007**) *Journal of Bacteriology* 189: 6176-6184.

[25] D. B. Steensgaard, H. Wackerbarth, P. Hildebrandt and A. R. Holzwarth (**2000**) *Journal of Physical Chemistry B* 104: 10379-10386.

[26] A. E. Bennett, C. M. Rienstra, M. Auger, K. V. Lakshmi and R. G. Griffin (**1995**) *Journal of Chemical Physics* 103: 6951-6958.

[27] A. E. Bennett, J. H. Ok, R. G. Griffin and S. Vega (**1992**) *Journal of Chemical Physics* 96: 8624-8627.

[28] I. de Boer, L. Bosman, J. Raap, H. Oschkinat and H. J. M. de Groot (**2002**) *Journal of Magnetic Resonance* 157: 286-291.

[29] A. Lange, S. Luca and M. Baldus (**2002**) *Journal of the American Chemical Society* 124: 9704-9705.

[30] B. J. van Rossum, H. Forster and H. J. M. de Groot (**1997**) *Journal Of Magnetic Resonance* 124: 516-519.

[31] S. Ganapathy, G. T. Oostergetel, P. K. Wawrzyniak, M. Reus, A. Gomez Maqueo Chew, F. Buda, E. J. Boekema, D. A. Bryant, A. R. Holzwarth and H. J. M. de Groot: *In Preparation*

[32] S. J. Ludtke, P. R. Baldwin and W. Chiu (**1999**) *Journal of Structural Biology* 128: 82-97.

[33] M. J. Frisch et al. (**2004**) Gaussian, Inc., Wallingford CT.

[34] A. D. Becke (**1986**) *Journal of Chemical Physics* 84: 4524-4529.

[35] C. T. Lee, W. T. Yang and R. G. Parr (**1988**) *Physical Review B* 37: 785-789.

[36] J. C. Facelli (**1998**) *Journal of Physical Chemistry B* 102: 2111-2116.

[37] Z. F. Chen, C. S. Wannere, C. Corminboeuf, R. Puchta and P. V. Schleyer (**2005**) *Chemical Reviews* 105: 3842-3888.

[38] R. Ditchfield (**1972**) *Journal of Chemical Physics* 56: 5688-5691.

[39] K. Wolinski, J. F. Hinton and P. Pulay (**1990**) *Journal of the American Chemical Society* 112: 8251-8260.

[40] R. Ditchfield (**1974**) *Molecular Physics* 27: 789-807.

[41] B. J. van Rossum, F. Castellani, K. Rehbein, J. Pauli and H. Oschkinat (**2001**) *Chembiochem* 2: 906-914.

[42] A. Egawa, T. Fujiwara, T. Mizoguchi, Y. Kakitani, Y. Koyama and H. Akutsu (**2007**) *Proceedings of the National Academy of Sciences of the United States of America* 104: 790-795.

[43] R. J. Abraham and A. E. Rowan (**1991**) *Nuclear magnetic resonance spectroscopy of chlorophyll*, (H. Scheer, Eds.) CRC Press, Boca Raton, FL.

[44] V. I. Prokhorenko, D. B. Steensgaard and A. R. Holzwarth (**2003**) *Biophysical Journal* 85: 3173-3186.

[45] K. Griebenow, A. R. Holzwarth, F. van Mourik and R. van Grondelle (**1991**) *Biochimica et Biophysica Acta* 1058: 194-202.

[46] L. A. Staehelin, J. R. Golecki and G. Drews (**1980**) *Biochimica et Biophysica Acta* 589: 30-45.

[47] T. P. Ikonen, H. Li, J. Psencik, P. A. Laurinmaki, S. J. Butcher, N. U. Frigaard, R. E. Serimaa, D. A. Bryant and R. Tuma (**2007**) *Biophysical Journal* 93: 620-628.

[48] D. B. Steensgaard, H. Wackerbarth, P. Hildebrandt and A. R. Holzwarth (**2000**) *Journal of Physical Chemistry B* 104: 10379-10386.

[49] T. Ishii, M. Kimura, T. Yamamoto, M. Kirihata and K. Uehara (**2000**) *Photochemistry and Photobiology* 71: 567-573.

[50] J. B. Arellano, M. Torkkeli, R. Tuma, P. Laurinmäki, T. B. Melø, T. P. Ikonen, S. J. Butcher, R. E. Serimaa and J. Pšenčík (**2008**) *Langmuir: the ACS journal of surfaces and colloids* 24: 2035-2041.

[51] S. A. Safran, P. A. Pincus, D. Andelman and F. C. Mackintosh (**1991**) *Physical Review A* 43: 1071-1078.

[52] I. de Boer, J. Matysik, M. Amakawa, S. Yagai, H. Tamiaki, A. R. Holzwarth and H. J. de Groot (**2003**) *Journal of the American Chemical Society* 125: 13374-5.